

### Correction of Aberrations of an Electron Microscope by Means of Electron Holography

Q. Fu, H. Lichte, and E. Völkl

*Institut für Angewandte Physik, Universität Tübingen, 7400 Tübingen 1, Germany*

(Received 21 May 1991)

Electron holography using the Möllenstedt-type electron biprism [G. Möllenstedt and H. Düker, *Z. Phys.* **145**, 377 (1956)] is now able to improve resolution and expressiveness of the electron microscope by subsequent correction of its aberrations and unique determination of amplitude and phase, as suggested by Gabor.

PACS numbers: 61.16.Di

Because of the interaction of the electrons with the specimen, the complex electron wave at the exit surface of an object, the object wave  $o(\mathbf{r})$ , is generally modulated both in amplitude  $a(\mathbf{r})$  and phase  $\varphi(\mathbf{r})$ . Therefore, it is possible to obtain information about the object from a highly magnified image of this object wave. Unfortunately, due to aberrations of the objective lens, the image wave  $b(\mathbf{r})$  with amplitude  $A(\mathbf{r})$  and phase  $\phi(\mathbf{r})$  is heavily distorted. In the case of the isoplanatic approximation, i.e., if the aberrations do not depend on  $\mathbf{r}$ , the image wave is given by

$$b(\mathbf{r}) = o(\mathbf{r}) * \text{PSF}(\mathbf{r}), \tag{1}$$

where  $*$  denotes convolution and  $\text{PSF}(\mathbf{r})$  is the point spread function caused by the aberrations of the microscope.

Preferably, the effect of the aberrations is described in the back focal plane of the objective lens. There, one finds the Fourier transform FT of the object wave  $o(\mathbf{r})$  multiplied by the “wave transfer function”  $\text{WTF}(\mathbf{q})$ ,

$$\text{FT}\{o(\mathbf{r})\} \text{WTF}(\mathbf{q}). \tag{2}$$

Performing the inverse Fourier transform of (2) one obtains the image wave (1). Obviously,  $\text{WTF} \equiv 1$  characterizes an ideal lens which uniquely transfers the amplitude and phase of the object wave  $o(\mathbf{r})$  into the amplitude and phase of the image wave  $b(\mathbf{r})$ . In order to discuss the effect of the wave transfer function,  $\text{WTF}(\mathbf{q})$  is usually written as

$$\text{WTF}(\mathbf{q}) = B(\mathbf{q}) e^{i\chi(\mathbf{q})}. \tag{3}$$

The pupil function  $B(\mathbf{q})$ , which damps the higher Fourier components of the object, can be defined by an aperture stop in the back focal plane of the objective lens, or can be caused by the “incoherent aberrations” induced by the illumination, i.e., by the limited spatial and temporal coherence in combination with the chromatic aberration of the objective lens.

The wave aberration  $\chi(\mathbf{q})$  acts like a phase plate in the Fourier plane. Its effect is to exchange the amplitude and phase of the object wave  $o(\mathbf{r})$  in a manner dependent on the spatial frequency  $\mathbf{q}$ , as sketched in Fig. 1.

With a suitable constant value for  $\chi$ , it would be possi-

ble to either direct the amplitude of the object wave  $o(\mathbf{r})$  into the amplitude of the image wave  $b(\mathbf{r})$  (for  $\chi \equiv 0$ ), or direct the phase of  $o(\mathbf{r})$  into the amplitude of  $b(\mathbf{r})$  ( $\chi \equiv \pi/2$  for  $|\mathbf{q}| \neq 0$ ; Zernike phase contrast). Although this is state of the art in light optics, it cannot be realized in electron microscopy, since  $\chi$  depends on the reciprocal-space vector  $\mathbf{q}$ .

In the isoplanatic approximation, the wave aberration  $\chi(\mathbf{q})$  is given by the “coherent” aberrations, e.g., axial astigmatism, spherical aberration, defocus, and axial coma. Whereas axial coma and axial astigmatism can be corrected by adjustment of the microscope, and defocus can be chosen by the operator, spherical aberration is a property of the objective lens which cannot be avoided [1]. Consequently, even at optimum adjustment of the electron microscope one has to deal with the wave aberration  $\chi$  given by

$$\chi(q) = \pi \Delta z \lambda q^2 + \frac{1}{2} \pi C_S \lambda^3 q^4, \tag{4}$$

where  $q = |\mathbf{q}|$ ,  $C_S$  is the coefficient of spherical aberration,  $\Delta z$  describes the defocus, and  $\lambda$  is the wavelength of the electrons.

By selection of a suitable defocus value, i.e., the “Scherzer focus” [2], and assuming the object to be a weak phase object, spherical aberration can be partially counterbalanced by defocus. A broad range of spatial frequencies is then transferred evenly at nearly the phase contrast condition  $\chi \approx \pi/2$  (Fig. 2). Nevertheless, the im-

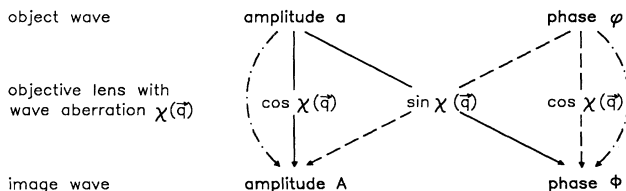


FIG. 1. Scheme of the transfer of a weakly modulated object wave into the image wave by means of an objective lens with wave aberration  $\chi(\mathbf{q})$ . The effect of  $\chi(\mathbf{q})$  is to distribute  $a$  and  $\varphi$  among  $A$  and  $\phi$  differently for different spatial frequencies  $\mathbf{q}$ , according to the transfer function  $\exp[i\chi(\mathbf{q})]$ ; therefore, the image is strongly disturbed. Ideal imaging corresponds to  $\chi \equiv 0$ .

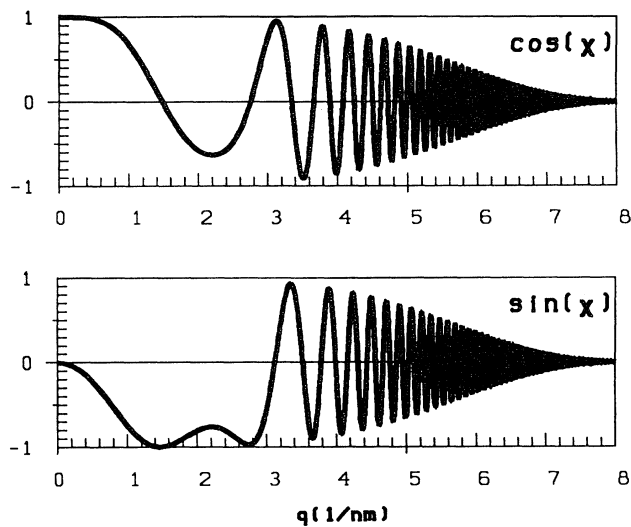


FIG. 2. Wave transfer function  $\exp[i\chi(q)] = \cos\chi(q) + i \times \sin\chi(q)$  including attenuation function at Scherzer focus. The point resolution is defined by the first zero of  $\sin\chi(q)$  at  $q = 3.1 \text{ nm}^{-1}$ ; the information limit at  $q = 6 \text{ nm}^{-1}$  is due to the damping by the incoherent aberrations below  $e^{-1}$ . Electron energy, 100 keV; energy width, 0.5 eV; coefficient of chromatic aberration,  $C_C = 1.2 \text{ mm}$ ; coefficient of spherical aberration,  $C_S = 1.2 \text{ mm}$ ; illumination aperture, 0.05 mrad.

age suffers from the following shortcomings: First, at Scherzer focus a broad range of spatial frequencies can be transferred, but no large-area phase contrast ( $q \rightarrow 0$ ) can be observed. This hampers, e.g., the imaging of biological specimen. Second, no real object is a pure weak phase object. Therefore, one finds in the image amplitude fragments of the object phase and the object amplitude mixed up. This "cross talk" inhibits a visual interpretation of the electron image in terms of the amplitude and the phase of the object, in particular, of objects with strong amplitude and phase components. This is true at any focus. Third, the cross talk is not reversible in conventional electron microscopy, since only the square of the image amplitude,  $A^2(r)$ , is recorded.

When using a modern field-emission gun, the spatial and temporal coherence improve remarkably. Therefore, the point resolution and information limit of the microscope have to be well distinguished (Fig. 2). As a result of the aberrations of the objective lens, the range between the point resolution and the information limit is lost for conventional imaging, because of the mixing between the object phase and amplitude. This range can be interpreted to some extent with the help of image simulation; however, it is made fully accessible by means of electron holography only.

Gabor realized that these problems can be overcome by electron holography, i.e., by recording the amplitude and the phase of the image wave [3]. Then, by subsequent deconvolution from  $\text{PSF}(r)$ , the image amplitude and

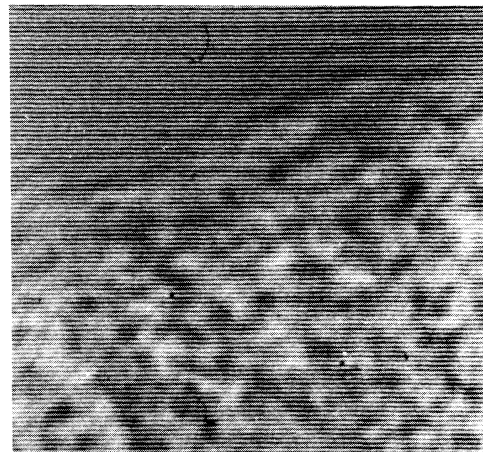


FIG. 3. Hologram of a carbon foil. The interference fringes with a spacing of 0.075 nm exhibit the phase and amplitude modulation of the image wave.

phase can be reordered and the object amplitude and phase displayed uniquely. There are two major steps involved in obtaining a reliable image. First, the microscope is used to collect all information in a hologram, i.e., the amplitude and the phase of the image wave  $b(r)$ , down to the information limit [4]. Second, the hologram is processed on the computer to retrieve the available information.

For recording a hologram, the image wave and a plane reference wave are superimposed at an angle by means of an electron biprism [5]. In the case of no aberrations, an

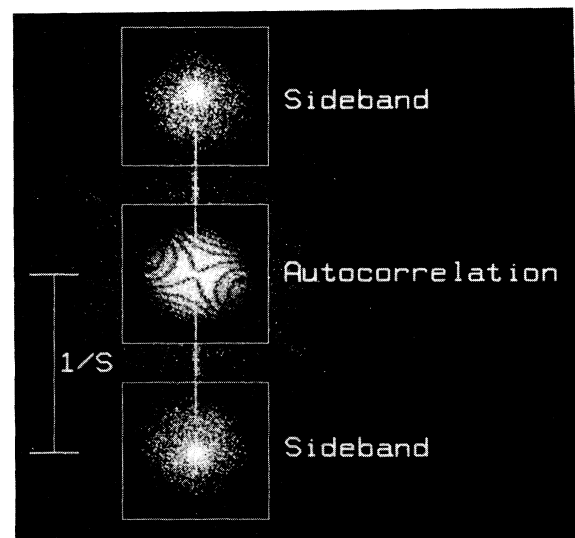


FIG. 4. Fourier transform of the hologram shown in Fig. 3. To avoid any overlap of the spectra, the distance  $1/s$  controlled by the fringe spacing  $s$  has to be sufficiently large.

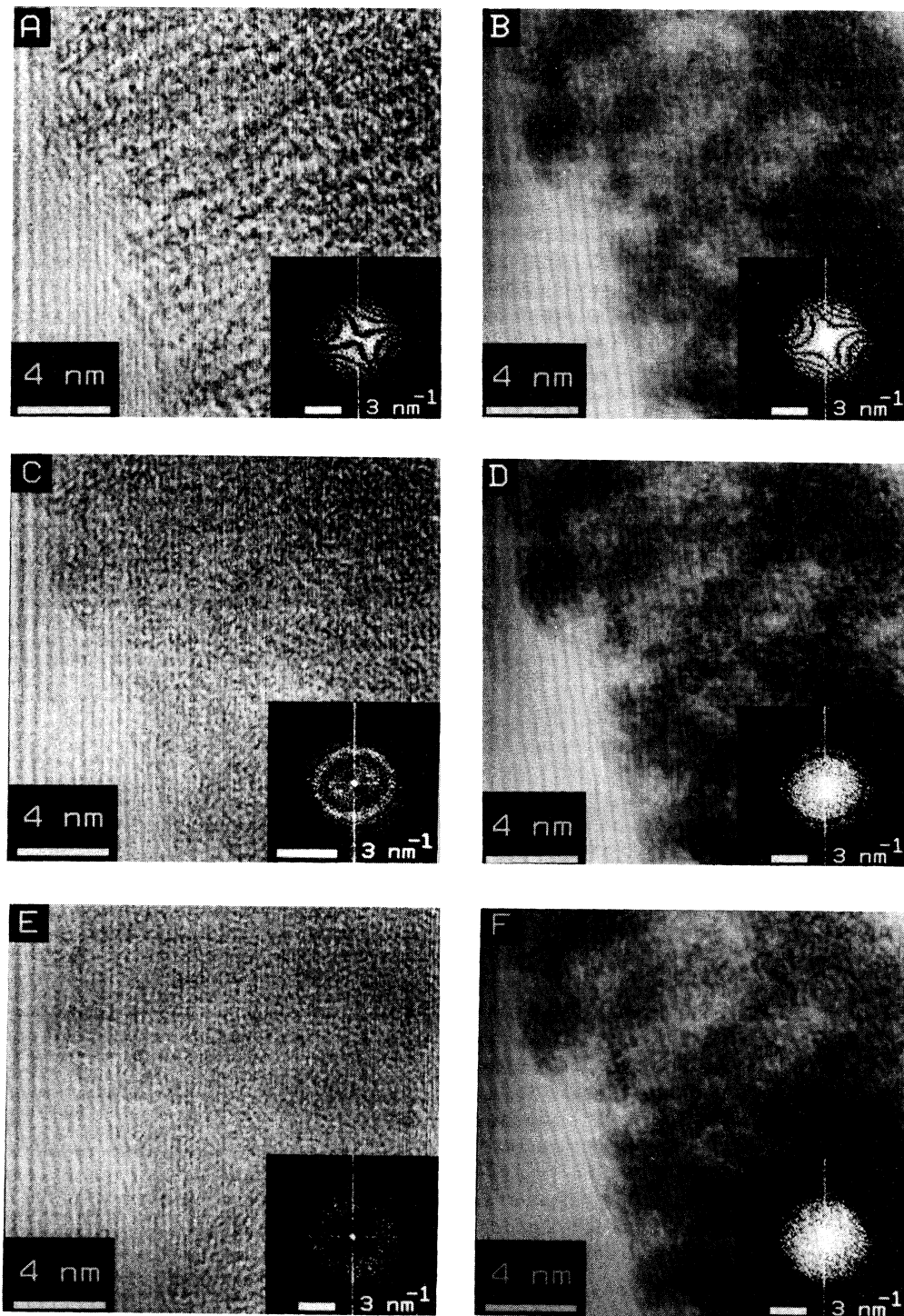


FIG. 5. The amplitude (left-hand side) and phase (right-hand side) of the wave reconstructed from a single hologram of carbon foil at different stages of correction of aberrations. Top, uncorrected; middle, corrected for astigmatism; bottom, corrected for astigmatism, spherical aberration, and defocus. The phase micrograph (f) represents carbon foil with the highest fidelity obtained so far in an electron microscope. Insets: the corresponding power spectra. The fringes on the left-hand side of each image stem from the Fresnel diffraction at the biprism filament. The streaks in the diffractograms could be avoided by Hanning windowing of the hologram prior to reconstruction.

interference pattern results given by

$$I(\mathbf{r}) = 1 + A^2(\mathbf{r}) + 2A(\mathbf{r})\cos[2\pi x/s + \phi(\mathbf{r})]. \quad (5)$$

The interference fringes are modulated in contrast  $2A(\mathbf{r})/[1 + A^2(\mathbf{r})]$  by the amplitude  $A(\mathbf{r})$  and in position by the phase  $\phi(\mathbf{r})$  of the image wave  $b(\mathbf{r})$  (Fig. 3).

Now the image wave has to be separated from the image intensity. This is done in Fourier space. The Fourier spectrum of Eq. (5) is shown in Fig. 4. The spectrum of the image intensity  $\text{FT}\{A^2(\mathbf{r})\}$  is convoluted around the  $\delta$  peak stemming from the 1 of Eq. (5), whereas the spectrum and the conjugate spectrum of the image wave  $\text{FT}\{b(\mathbf{r})\}$  are convoluted around the two  $\delta$  peaks from the cosine term in Eq. (5), respectively. In order to avoid any overlap between  $\text{FT}\{A^2(\mathbf{r})\}$  and  $\text{FT}\{b(\mathbf{r})\}$ , the fringe spacing  $s$  has to be smaller than the smallest period in the image wave by a factor of 2 to 3.

The fine fringe spacing  $s$  needed at high resolution challenges the stability of the microscope: Using a Philips EM 420 electron microscope with a field-emission gun, equipped with an electron biprism and carefully refined for the special needs, we routinely take holograms with a fringe spacing as narrow as 0.05 nm [6]. Meanwhile, we have even succeeded in taking holograms with a fringe spacing of  $\frac{1}{30}$  nm, allowing us to collect all the information about the amplitude and phase needed for a point resolution of 0.1 nm after correction [7].

For the reconstruction of the object wave from the hologram, we apply the methods of numerical image processing [6,8]: The hologram is digitized at  $4096 \times 4096$  sampling points and fed into a computer. After Fourier transformation, the spectrum  $\text{FT}\{b(\mathbf{r})\}$  of the image wave is extracted as a subimage; apart from the incoherent attenuation function, it agrees with the spectrum of the object wave found in the electron microscope multiplied by the wave aberration  $\exp[i\chi(\mathbf{q})]$ . Next, a numerical phase plate  $\exp[-i\chi(\mathbf{q})]$  is applied to annihilate  $\exp[i\chi(\mathbf{q})]$  and hence to correct for astigmatism, spherical aberration, and defocus. Finally, the inverse Fourier transform renders the aberration-free object wave which can be displayed by amplitude and phase at arbitrary focus. Presently, this reconstruction procedure takes somewhat more than 1 h; however, the first real time reconstructions have already been shown [9].

In Figs. 5(a)–5(f) the effects of correction of aberrations at high resolution are demonstrated for the first time. We have selected amorphous carbon foil as an ob-

ject which provides all relevant spatial frequencies. The hologram was intentionally taken with some axial astigmatism to show the effect of its holographic correction. The amplitude (a) and phase (b) reconstructed without any correction reveal some strong astigmatism as indicated by the lack of rotational symmetry in the respective power spectra. Astigmatism disappears in the amplitude (c) and phase (d) after application of a corresponding phase plate. Now the spectra show rotational symmetry but dark and bright rings indicate the presence of spherical aberration and defocus. These, too, disappear after application of the respective phase plate; as to be expected at ideal imaging of a weak phase object, the object structure is predominantly found in the reconstructed phase (f) rather than in the amplitude (e). The phase micrograph (f) shows the carbon foil in an improved way in that it represents the spatial frequencies ranging from 0 to approximately  $4 \text{ nm}^{-1}$ . In particular, the strong large-area phase contrast changes the appearance of the foil drastically compared to conventional micrographs. The upper limit at about  $4 \text{ nm}^{-1}$  will be overcome by improving both the stability of the microscope and the precision of the determination of  $C_S$  and  $\Delta z$ . All previously presented micrographs look similar to the amplitude micrograph (c) which contains too many optical artifacts to be representative of the real object because the various spatial frequencies of which it is composed have been transferred with widely varying transfer factors.

Thanks are due to Körberstiftung, Volkswagenstiftung, and Deutsche Forschungsgemeinschaft for financial support.

- 
- [1] O. Scherzer, *Z. Phys.* **101**, 593 (1936).
  - [2] O. Scherzer, *J. Appl. Phys.* **20**, 20 (1949).
  - [3] D. Gabor, *Nature (London)* **161**, 777 (1948).
  - [4] H. Lichte, *Ultramicroscopy* (to be published).
  - [5] H. Wahl, thesis, Universität Tübingen, 1975 (unpublished).
  - [6] H. Lichte, *Adv. Opt. Electron Microsc.* **12**, 25 (1991).
  - [7] E. Völkl und H. Lichte, *Ultramicroscopy* **32**, 177 (1990).
  - [8] F.-J. Franke, K.-H. Herrmann, and H. Lichte, *Scanning Microsc. Suppl.* **2**, 59 (1988).
  - [9] W. D. Rau, H. Lichte, E. Völkl, and U. Weierstall, "Real Time Reconstruction of Electron Off-Axis Holograms Recorded with a High Pixel CCD Camera" (to be published).

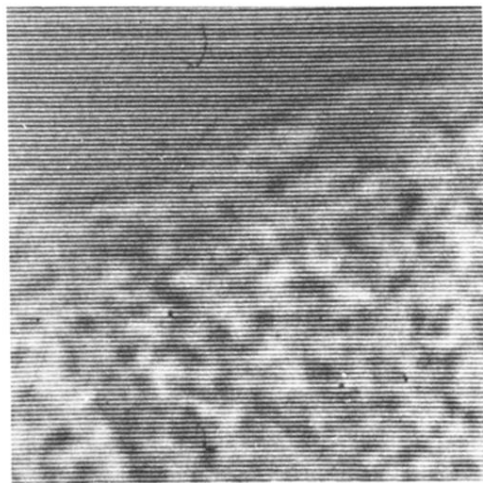


FIG. 3. Hologram of a carbon foil. The interference fringes with a spacing of 0.075 nm exhibit the phase and amplitude modulation of the image wave.

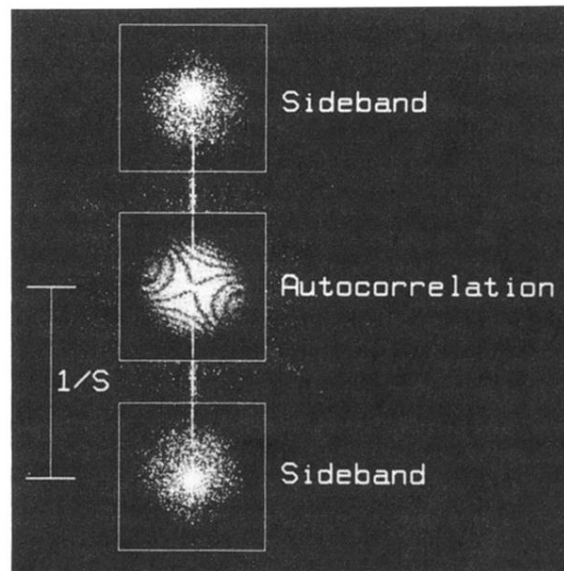


FIG. 4. Fourier transform of the hologram shown in Fig. 3. To avoid any overlap of the spectra, the distance  $1/s$  controlled by the fringe spacing  $s$  has to be sufficiently large.

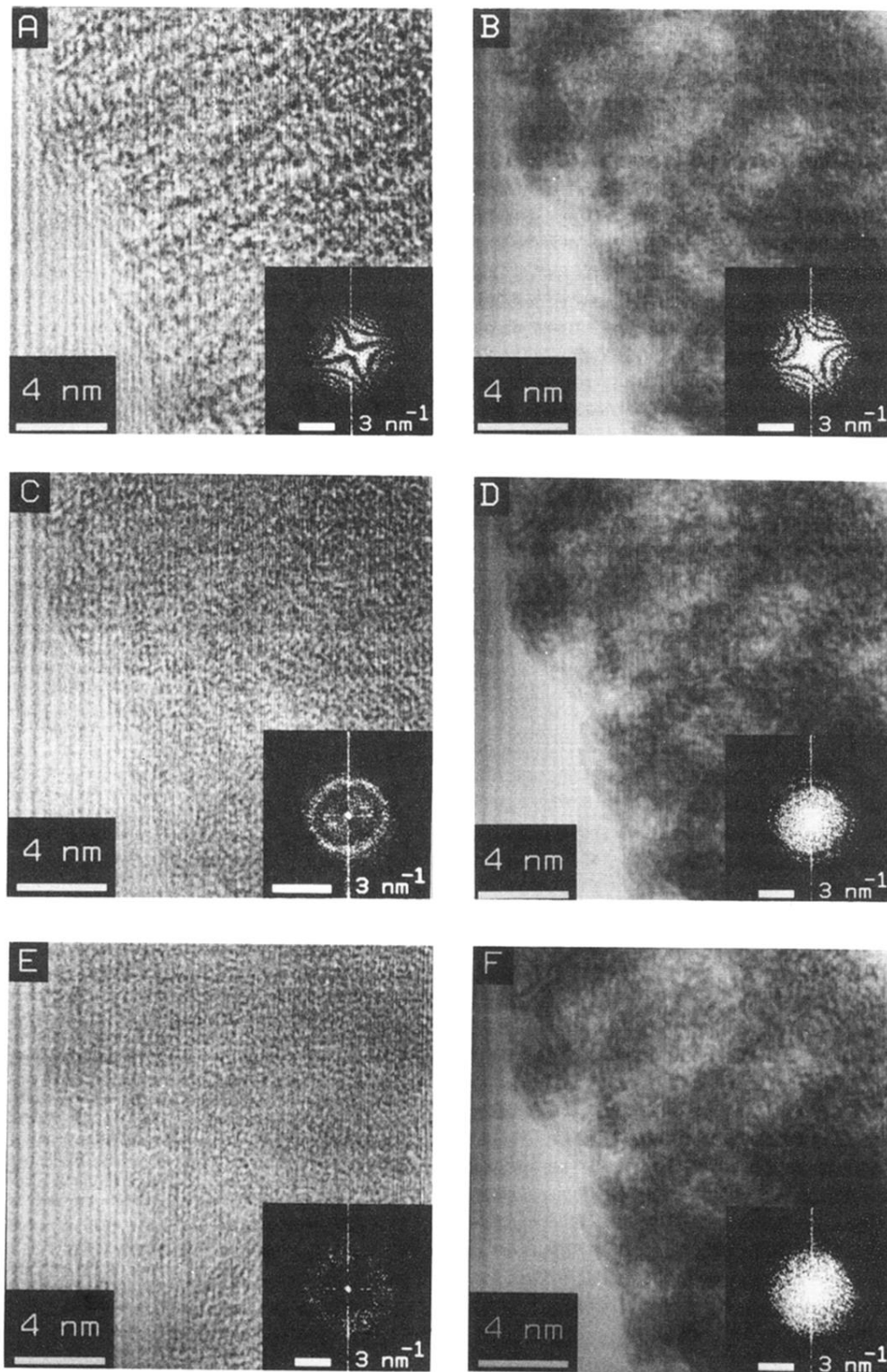


FIG. 5. The amplitude (left-hand side) and phase (right-hand side) of the wave reconstructed from a single hologram of carbon foil at different stages of correction of aberrations. Top, uncorrected; middle, corrected for astigmatism; bottom, corrected for astigmatism, spherical aberration, and defocus. The phase micrograph (f) represents carbon foil with the highest fidelity obtained so far in an electron microscope. Insets: the corresponding power spectra. The fringes on the left-hand side of each image stem from the Fresnel diffraction at the biprism filament. The streaks in the diffractograms could be avoided by Hanning windowing of the hologram prior to reconstruction.